PROCEEDINGS OF SCIENCE

Pion structure from lattice QCD

G. Bali, S. Collins, B. Glässle, M. Göckeler, N. Javadi-Motaghi*, J. Najjar, W. Söldner, A. Sternbeck

Institut für Theoretische Physik, Universität Regensburg, 93040 Regensburg, Germany

E-mail: Narjes.Javadi-Motaghi@physik.uni-regensburg.de

We report on the lowest moment of parton distribution functions and generalized form factors for the pion at several values of the momentum transfer. Calculations are performed for $N_f = 2$ flavors of $\mathcal{O}(a)$ improved Wilson fermions with pion masses down to 150 MeV.

31st International Symposium on Lattice Field Theory - LATTICE 2013
July 29 - August 3, 2013
Mainz, Germany

*Speaker.

PoS(LATTICE 2013)447

1. Introduction

The pion plays a central role in many problems of strong interaction physics. It is the lightest hadronic bound state, with two (up and down) valence quarks and spin zero, and there is one neutral (π^0) and two charged pions ($\pi^\pm$). Pions are produced in hadronic collisions at high-energies, for example, in the Earth's atmosphere due to cosmic rays, but pions decay also very quickly, either electromagnetically or weakly (e.g., $\pi^0 \to 2\gamma$ or $\pi^- \to \mu^- + \bar{\nu}_\mu$).

The inner structure of pions has been studied experimentally to some extent. Among the experimentally measured quantities is the electromagnetic form factor F_π (see, e.g., [1])

$$\langle \pi(\vec{p}')|J^\mu_{em}(\vec{p}'-\vec{p})|\pi(\vec{p})\rangle = (p'+p)^\mu F_\pi(t) \qquad \text{with} \quad t \equiv \Delta^2 = (p'-p)^2 \tag{1.1}$$

where p and p' are the incoming and outgoing momenta and t is the momentum transfer. F_π describes the charge distribution of a pion, that is the deviation of a pion from being a point-like charge interacting with the electromagnetic field.

Another quantity is the pion parton distribution function (PDF) $f_\pi(x)$. It describes the distribution of the momenta of the quarks and gluons (partons) inside the pion. For each parton it is a function of the longitudinal momentum fraction x carried by the parton. Experimentally, PDFs can be accessed, for example, for larger x via a Drell-Yan process $\pi^\pm N \to \mu^+\mu^- X$ (see, e.g., [2]) or a prompt photon production process, $\pi^+ p \to \gamma X$ [3].

In modern language hadron structure is expressed in terms of generalized parton distributions (GPDs). These contain the electromagnetic form factor and parton distribution functions as limiting cases, but more importantly provide also information on the partonic content as a function of both the longitudinal momentum fractions and the total momentum transfer. At leading twist there is one vector GPD and one tensor GPD for the pion, $H^\pi(x,\xi,t)$ and $E^\pi_T(x,\xi,t)$.

Lattice QCD allows us to determine the space-like pion electromagnetic form factor from first principles (see, e.g., [4] for a recent review). In contrast, pion PDFs or GPDs are not accessible directly. Their Mellin moments are, however. For example, $\langle x\rangle^\pi = \int_{-1}^1 dx\, x f_\pi(x)$ or

$$\int_{-1}^1 dx\, H^\pi(x,\xi,t) = A^\pi_{1,0}(t) \quad \text{and} \quad \int_{-1}^1 dx\, x H^\pi(x,\xi,t) = A^\pi_{20}(t) + (-2\xi)^2 C^\pi_{20}(t)\,, \tag{1.2}$$

where the coefficients A and C (also known as the generalized form factors of the pion) are real functions of the momentum transfer t and the renormalization scale μ. These can be estimated on the lattice from expectation values of local operators, because, for the above examples,

$$\langle \pi(\vec{p}')|\hat{\mathcal{O}}^\mu_V(0)|\pi(\vec{p})\rangle = 2\bar{P}^\mu A^\pi_{1,0}(t) \tag{1.3}$$

$$\langle \pi(\vec{p}')|\hat{\mathcal{O}}^{\mu\mu_1}_V(0)|\pi(\vec{p})\rangle = 2\bar{P}^\mu \bar{P}^{\mu_1} A^\pi_{2,0}(t) + 2\Delta^\mu \Delta^{\mu_1} C^\pi_{2,0}(t) \tag{1.4}$$

with $\mathcal{O}^{\mu_1\cdots\mu_n}_q = \bar{q}\gamma^{\{\mu} i\overleftrightarrow{D}^{\mu_1}\cdots i\overleftrightarrow{D}^{\mu_n\}} q$ – trace being the traceless part of a quark bilinear, $\bar{P}^\mu = (p'^\mu + p^\mu)/2$, and q and $\bar{q}$ denoting the quark fields. It is clear that in this framework $F^\pi(t) = A^\pi_{1,0}(t)$ and $\langle x\rangle^\pi = A^\pi_{2,0}(t=0)$.

2. Lattice calculations

In this contribution we provide new data for $\langle x\rangle^\pi$, F_π, $A^\pi_{2,0}$ and $C^\pi_{2,0}$. In our calculations, we use the non-perturbatively improved Sheikholeslami-Wilson fermion action with two mass-degenerate

β	κ	Volume	#cfg $\times M$	a[fm]	m_π [MeV]	$m_\pi L$	t_{sink}/a
5.29	0.13620	$24^3 \times 48$	1170×2	0.07	430	3.7	24
	0.13620	$32^3 \times 64$	2000×2		422	4.8	32
	0.13632	$32^3 \times 64$	967×1		294	3.4	32
	0.13632	$40^3 \times 64$	2028×2		289	4.2	32
	0.13640	$48^3 \times 64$	722×2		157	2.7	32
	0.13640	$64^3 \times 64$	1238×3		150	3.5	32
5.40	0.13640	$32^3 \times 64$	1124×2	0.06	491	4.8	32
	0.13660	$48^3 \times 64$	2178×2		260	3.8	32

Table 1: Parameters for our lattice calculations. M is the number of sources per configuration; the sink-source separation is $t_{sink} = L_t/2$. The pion masses quoted were obtained on the respective finite volumes.

flavors of sea quarks and the Wilson plaquette action. For the lattice couplings we use $\beta = 5.29$ and 5.40, which correspond to lattice spacings of about 0.07 fm and 0.06 fm, respectively. For each β we use different values for κ to cover a range of pion mass values (see Table 1). The lowest pion mass we reach is about 150 MeV and the largest 490 MeV. For each set of parameters, we have analyzed about 700–2000 gauge configurations and on each configuration, data was taken for one, two or three sources, depending on the parameters (see Table 1). The first source (per configuration) is chosen at a random spacetime position. The remaining ones are placed with maximal distance between them. To convert our data to physical units we assume a Sommer scale of $r_0 = 0.5$ fm [5] and use non-perturbative renormalization constants for the conversion to the $\overline{\text{MS}}$ scheme [6].

To extract the matrix elements for the various local operators, we use appropriate ratios of three- and two-point functions (see, e.g., [7])

$$R(t_{sink}, \tau, p', p) = \frac{C^{\mathscr{O}}_{3pt}(\tau, \vec{p}', \vec{p})}{C_{2pt}(t_{sink}, \vec{p}')} \sqrt{\frac{C_{2pt}(t_{sink} - \tau, \vec{p}) C_{2pt}(\tau, \vec{p}') C_{2pt}(t_{sink}, \vec{p}')}{C_{2pt}(t_{sink} - \tau, \vec{p}') C_{2pt}(\tau, \vec{p}) C_{2pt}(t_{sink}, \vec{p})}} \,. \tag{2.1}$$

For large $\tau \ll t_{sink}$ these ratios saturate to a constant which we determine by a fit over several τ (see, e.g., Figure 1). Here $C_{2pt}(t, \vec{p})$ denotes the pion two-point function with a pion creation operator at the Euclidean time t_1 and an annihilation operator at $t_2 = t_1 + t$. $C^{\mathscr{O}}_{3pt}(\tau, \vec{p}', \vec{p})$ refers to a pion three-point function with a current insertion (operator $\mathscr{O}$) at $t_1 + \tau < t_2$. Since for the particular case of a pion we can set $t_{sink} = L_t/2$, we can average over forward and backward propagating pions, which reduces the statistical noise. Also $\mathscr{O}$ can be placed far away from sink and source which suppresses contributions from excited states by factors of $e^{-\Delta E \tau}$ and $e^{-\Delta E (\tau - t_{sink})}$.

For the calculation of the two and three-point functions we use the Chroma software package [8]. The three-point functions are obtained via the sequential-source technique, with an improved sink- and source-smearing to reduce excited-state contaminations (see [9] for details). Although additional calculations are currently being performed for the disconnected diagrams, here we only report on the connected contributions.

3. Results

The effectiveness of our sink-source smearing is demonstrated in Figure 1. There we show

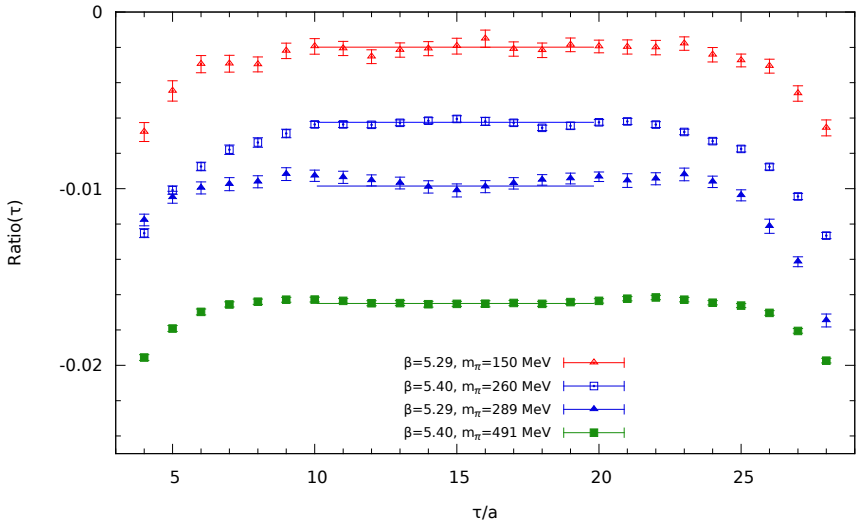

Figure 1: Ratios at sink-source separation $L_t/2$ for the operator $O^{(\vec{p}=0)}_{v_{2,b}}$ for different pion masses and lattice spacings.

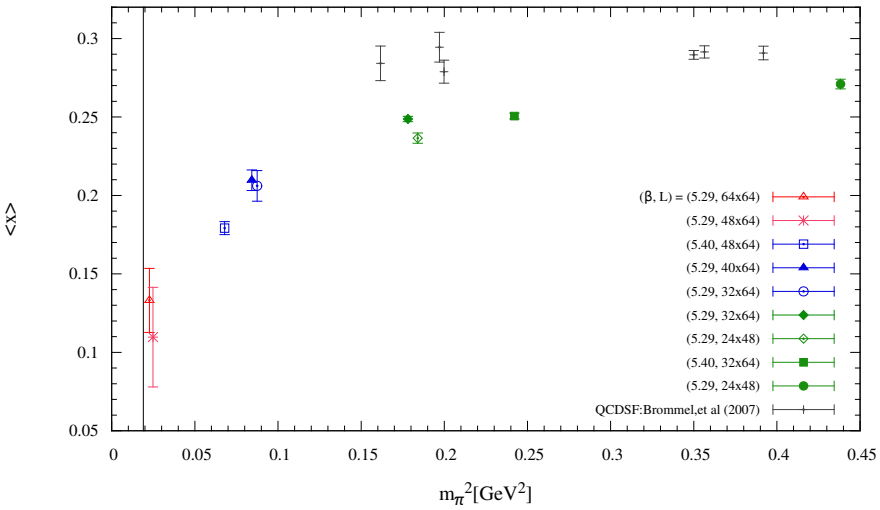

Figure 2: First moment of the pion PDF in the $\overline{\text{MS}}$ scheme, $\langle x\rangle_{u-d}$ without disconnected contributions. Solid symbols are for $m_\pi L > 4$, open symbols for $m_\pi L > 3$ and the star for $m_\pi L < 3$. Gray plus symbols are from [10]. The vertical solid line marks the position of the physical pion mass.

ratios for the operator[1] $O_{v_{2,b}}$ with vanishing $\vec{p} = \vec{p}'$, which one needs for instance for $\langle x\rangle^\pi$. Data are shown for different lattice spacings and pion masses, and although the latter vary quite a bit, we find for all these sets long plateaus which can safely be fitted to constants.

Note that the symbol colors in Figure 1 are chosen according to the pion mass: Red symbols are used for data for the lightest pion mass ($m_\pi \approx 150\,\text{MeV}$), blue symbols for the second lightest mass ($m_\pi \approx 260 - 290\,\text{MeV}$) and green symbols for pion masses above 400 MeV. The same color scheme also applies to the other figures.

[1] For the operator labeling we follow the notation of [11].

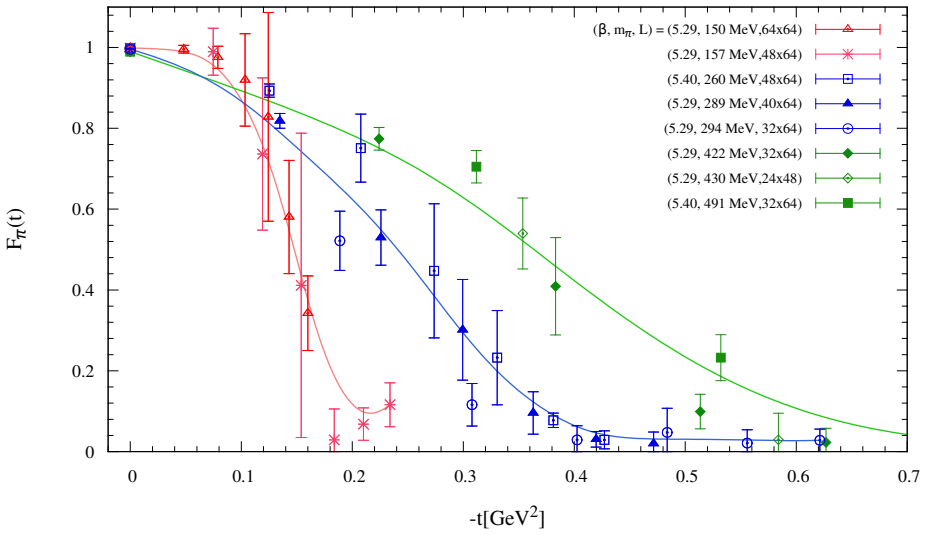

Figure 3: Pion electromagnetic form factor for $150\,\text{MeV} \leq m_\pi \leq 495\,\text{MeV}$. Splines are to guide the eyes.

From the ratios for $O_{v_{2,b}}$ we can estimate the connected contributions to $\langle x \rangle^\pi$. In Figure 2 we show our current (preliminary) data for the available pion mass range. To underpin the effect of our improved sink-source smearing we also show there results from [10]. Those results were partly obtained on the same gauge ensembles but for a different type of smearing. A comparison shows, there is a systematic deviation between those old and our new data. Our results lie systematically below those of [10] and this deviation increases with decreasing m_π. This suggests that with our improved sink-source smearing technique we have a much better control over excited-state contributions [9].

Besides $\langle x \rangle^\pi$ we are also interested in the form factors. In Figure 3 we show our current estimates for the electromagnetic form factor $F_\pi(t)$ versus $-t = (p - p')^2$. Data points are shown for three different pion masses and these clearly demonstrate the m_π dependence of $F_\pi(t)$. Our data at small $|t|$ also show the flattening of points for $t \to 0$, which was seen in [12]. In comparison to $\langle x \rangle^\pi$ our data for $F_\pi(t)$ is however quite noisy. A reason could be setting $t_{sink} = L_t/2$. This is certainly the best choice for $\langle x \rangle^\pi$, but for finite momentum transfer a smaller t_{sink} would perhaps have been the better choice. This certainly deserves further study.

In Figure 4 we also show first data for some generalized pion form factors. These currently come with even larger statistical uncertainties than we see for the electromagnetic form factor. A pion mass dependence for A_{20}^π is seen nonetheless. In the limit $t \to 0$ this dependence is of course the same as we saw in Figure 2, but it seems to persist also for larger $|t|$.

4. Conclusions

We have presented an update on our effort towards a precise understanding of the structure of pions based on lattice QCD calculations. These are performed for two dynamical Clover-Wilson fermion flavors for pion masses ranging from 490 MeV down to 150 MeV. Here we have reported on our new data for the connected contribution to the lowest moment of quark distribution functions $\langle x \rangle^\pi$ and also shown some (preliminary) results for the generalized form factors, namely for F_π,

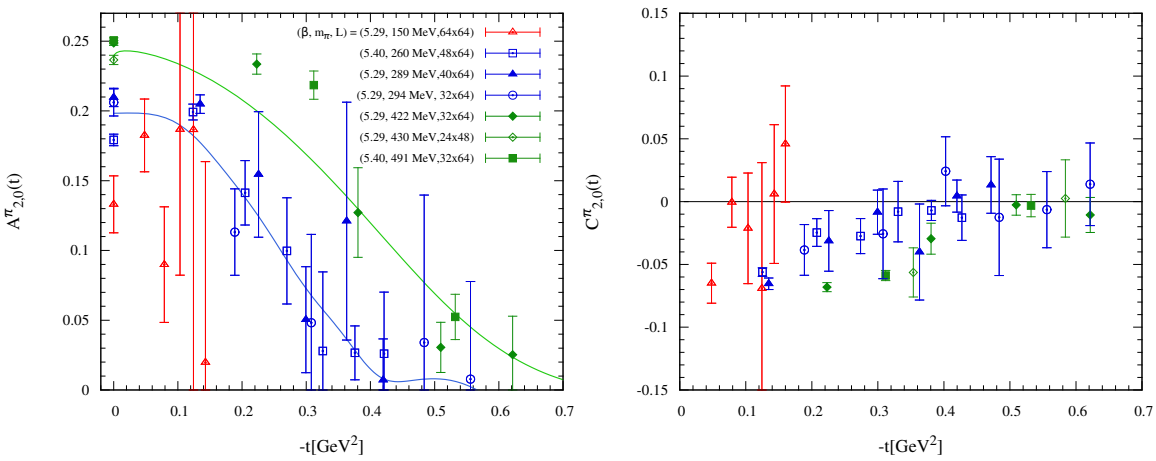

Figure 4: Preliminary results for the generalized form factors A_{20} and C_{20} versus momentum transfer $-t$. Symbols and colors have the same meaning in both panels.

A_{20} and C_{20}. We find that values for $\langle x \rangle^\pi$ obtained with our improved smearing lie well below the corresponding older data [13] (without this smearing). In contrast to these, we also see a non-linear m_π^2-dependence for $\langle x \rangle^\pi$. This raises the question up to what pion masses leading order chiral perturbation theory (as given, e.g., in [14]) is applicable.

Also for F_π and A_{20} we are able to reveal a clear pion mass dependence (see Figs. 3 and 4). Unfortunately, our resolution at small $|t|$ is not as optimal as it is with twisted boundary conditions (as performed, e.g., in [12]). Nevertheless, we see a similar flattening of points for F_π for small $|t|$. To reduce the statistical noise, we plan to reconsider our choice of $t_{sink} = L_t/2$. This results in clear plateaus for ratios R at zero momentum transfer but for finite momentum transfer, as needed for the form factors, the noise increases with $|t|$.

More details and additional data will be presented in a forthcoming article.

Acknowledgements

Calculations have been performed on the SuperMUC system at the LRZ (Munich, Germany). We have made use of the Chroma software suite [8] adapted for our needs. This work has been supported in parts by the DFG (SFB/TR 55, Hadron Physics from Lattice QCD) and the EU under grant 238353 (ITN STRONGnet). N.M-J. and A.St. acknowledge support by the European Reintegration Grant (FP7-PEOPLE-2009-RG, No.256594).

References

[1] C. Bebek *et al.*, Phys.Rev. **D17**, 1693 (1978); H. Ackermann *et al.*, Nucl.Phys. **B137**, 294 (1978); S. Amendolia *et al.* (NA7 Collaboration), Nucl.Phys. **B277**, 168 (1986); T. Horn *et al.* (Jefferson Lab F(pi)-2 Collaboration), Phys.Rev.Lett. **97**, 192001 (2006); G. Huber *et al.* (Jefferson Lab), Phys.Rev. **C78**, 045203 (2008).

[2] J. Badier *et al.* (NA3 Collaboration), Z.Phys. **C18**, 281 (1983); B. Betev *et al.* (NA10 Collaboration), Z.Phys. **C28**, 15 (1985); P. Aurenche *et al.*, Phys.Lett. **B233**, 517 (1989); M. Bonesini

et al. (WA70 Collaboration), Z.Phys. **C37**, 535 (1988); J. Conway *et al.*, Phys.Rev. **D39**, 92 (1989).

[3] P. J. Sutton *et al.*, Phys. Rev. D **45**, 2349 (1992).

[4] B. B. Brandt, arXiv:1310.6389 [hep-lat].

[5] G. Bali *et al.*, Nucl.Phys. **B866**, 1 (2013), arXiv:1206.7034 [hep-lat].

[6] M. Göckeler *et al.*, Phys.Rev. **D82**, 114511 (2010), arXiv:1003.5756 [hep-lat].

[7] P. Hägler, Phys.Rept. **490**, 49 (2010), arXiv:0912.5483 [hep-lat].

[8] R. G. Edwards and B. Joó (SciDAC Collaboration, LHPC Collaboration, UKQCD Collaboration), Nucl.Phys.Proc.Suppl. **140**, 832 (2005), arXiv:hep-lat/0409003 [hep-lat].

[9] G. Bali *et al.*, PoS **Lattice2013**, 290 (2013), these proceedings.

[10] D. Brömmel, *Pion Structure from the Lattice*, Ph.D. thesis, Institute for Theoretical physic, University of Regensburg,Germany (2007).

[11] M. Göckeler *et al.*, Phys.Rev. **D54**, 5705 (1996), arXiv:hep-lat/9602029 [hep-lat].

[12] B. B. Brandt, A. Jüttner, and H. Wittig, arXiv:1306.2916 [hep-lat].

[13] D. Brömmel *et al.* (QCDSF-UKQCD Collaboration), PoS **LAT2007**, 140 (2007).

[14] M. Diehl, A. Manashov, and A. Schäfer, Phys.Lett. **B622**, 69 (2005), arXiv:hep-ph/0505269 [hep-ph].